Chinese Journal of Chemical Engineering 26 (2018) 81–88

Contents lists available at ScienceDirect

Chinese Journal of Chemical Engineering

journal homepage: www.elsevier.com/locate/CJChE

Article

# Hierarchical pore structure of activated carbon fabricated by $CO_2$/microwave for volatile organic compounds adsorption☆

Wenjuan Qiu [1], Kang Dou [1], Ying Zhou [2], Haifeng Huang [1], Yinfei Chen [2], Hanfeng Lu [2,*]

[1] College of Environment, Zhejiang University of Technology, Hangzhou 310014, China
[2] College of Chemical Engineering, Zhejiang University of Technology, Hangzhou 310014, China

ARTICLE INFO

*Article history:*
Received 5 January 2017
Received in revised form 1 April 2017
Accepted 8 April 2017
Available online 27 April 2017

*Keywords:*
Activated carbon
$CO_2$/microwave
Pore regulation
volatile organic compounds
Desorption

ABSTRACT

An activated carbon pore-expanding technique was achieved through innovative reactivation by $CO_2$/microwave. The original and modified activated carbons were characterized by nitrogen adsorption–desorption, scanning electron microscopy, transmission electron microcopy, and Fourier transform infrared spectroscopy. The mesopore volume increased from 0.122 $cm^3 \cdot g^{-1}$ to 0.270 $cm^3 \cdot g^{-1}$, and a hierarchical pore structure was formed. A gradual decrease in the phenolic hydroxyl and carboxyl groups on the surface of activated carbon enhanced the surface inertia of granular activated carbon (GAC). The toluene desorption rate of the modified sample increased by 8.81% compared with that of the original GAC. Adsorption isotherm fittings revealed that the Langmuir model was applicable for the original and modified activated carbons. The isosteric adsorption heat of toluene on the activated carbon decreased by approximately 50%, which endowed the modified sample with excellent stability in application. The modified samples showed an enhanced desorption performance of toluene, thereby opening a way to extend the cycle life and improve the economic performance of carbon adsorbent in practical engineering applications.


## 1. Introduction

In commonly used adsorbents, activated carbon is the most extensive porous adsorption material [1,2]. The application of activated carbon involves liquid and gas phase separation in food, catalysis, medicine, energy storage, and many other national economic fields [3–6]. Activated carbon, as an efficient and economical adsorbent, has been recently used for the adsorption removal of environmental pollutants, particularly for the adsorption treatment process of volatile organic compounds (VOCs) [7], and occupies most of the market application space [8,9]. Some novel carbon-based adsorption materials, such as activated carbon fiber and super active carbon (*i.e.*, $S_{BET}$ > 2000 $m^2 \cdot g^{-1}$), emerge as the times require [10,11].

At the macroscopic level, the adsorption capacity of activated carbon is determined by specific surface area, pore structure, surface properties, and adsorbate properties. From the microscopic view, the adsorption of activated carbon is mainly determined by the physical adsorption of van Edward force and the role of micropore filling and capillary condensation. Activated carbon is a typical micro-mesoporous structure adsorbent. Strong adsorption potential and high adsorption capacity are generated in the micropore-filling mechanism because the molecular size of the micropore and the adsorbate is of the same order of magnitude. Mesopores provide channels for the adsorbate molecules into the micropores and rich adsorption sites. The desorption of adsorbed molecules on the surface of activated carbon is an inverse process of adsorption, and the desorption performance is directly related to the cycle life of the activated carbon and the cost of the material. However, an unsuitable pore structure (as shown in Fig. 1(a): ink bottle-type hole ①, tapered hole ②, and beaded hole ③) will cause high diffusion resistance and strong surface adsorption, which significantly increase the resistance of desorption and make it difficult for some adsorbed molecules to be removed and retained in the pores of activated carbon. Moreover, the strong adsorption potential induced by abundant surface active groups causes the heat release to increase during adsorption process, which will lead to a sudden rise in the temperature of the adsorbent bed and cause safety accidents and even explosion. Given the unfavorable desorption performance and the thermal stability, the cycle life of activated carbon is shortened [12]. Therefore, this study focused on the secondary regulation of the pore structure of activated carbon to expand pore size (as shown in Fig. 1 ①–①′, ②–②′, and ③–③′) and reduce the surface activity by microwave-induced $CO_2$ activation to improve its desorption performance and the thermal stability.

☆ Supported by the National Natural Science Foundation of China (21506194, 21676255), the Natural Science Foundation of Zhejiang Province (Y16B070025), the Commission of Science and Technology of Zhejiang Province (2013C03021, 2017C33106).
* Corresponding author.
*E-mail address:* luhf@zjut.edu.cn (H. Lu).

http://dx.doi.org/10.1016/j.cjche.2017.04.006
1004-9541/

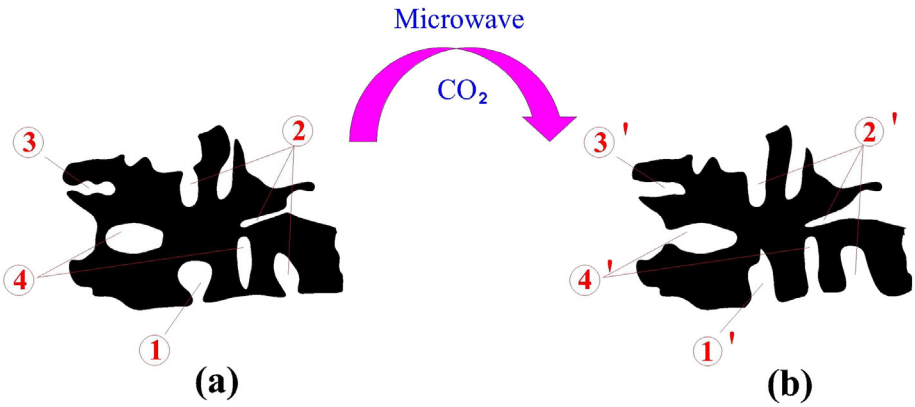


**Fig. 1.** Schematic model for pore structure of the activated carbon before (a) and after (b) $CO_2$/microwave modification.

Previous researches showed that catalyzing the steam activation process by using transition metals or rare earth metal compounds was verified to be one of the most effective approaches for increasing mesopore volume of activated carbon [13–15]. Recently, KOH and $H_3PO_4$ as cheap and effective activating agents were exploited as catalysts for the steam activation to regulate the pore size distribution of activated carbon [16,17]. The preparation of activated carbon typically includes two steps of high-temperature carbonization and activation. In the process of high-temperature activation, compared with the traditional heating method of heat conduction, microwave heating, with its characteristics of fast heating speed, small temperature gradient, and high energy utilization rate, is increasingly used as the energy source. Microwave chemistry has been widely used in preparing and modifying activated carbon in recent years [18–20]. $CO_2$ is a pore-forming agent commonly used in the physical activation process of activated carbon preparation at elevated temperatures [21,22]. In this study, we selected $CO_2$ as the etching gas to react with the carbon atoms in the active position and the surface active groups of the carbon material to form and expand the pore structure [23]. Innovative microwave-induced carbon dioxide modification on commercial activated carbon was then formed.

In this study, a commercial coal-based granular activated carbon (GAC) was selected as the raw material. Under the atmosphere of pure $CO_2$ and microwave irradiation power of 0.8 kW, the activation time was taken as the experimental variable to conduct the reactivation modification of activated carbon. The physical and chemical properties of the modified activated carbon were characterized by specific surface area and pore size analysis, scanning electron microscopy (SEM), transmission electron microscopy (TEM), Fourier transform infrared (FTIR) spectroscopy, and water contact angle. The adsorption–desorption performance and isosteric adsorption heat of activated carbon were investigated before and after modification.

This study aims to (1) design a modification method of pore expansion and surface inertia on commercial activated carbon; (2) investigate the effect of modification on the GAC by $CO_2$/microwave technique; and (3) examine the desorption properties and the thermal effect of adsorption by controlling the pore structure and surface properties.

## 2. Experimental

### 2.1. $CO_2$/microwave modification

10 g of commercial coal-based activated carbon (Shanghai Quanhu Active Carbon Co., Ltd.) was weighed and placed in boiling water to boil for 30 min to remove ash and other adsorbed impurities. Subsequently, the sample was washed with deionized water several times until the supernatant became clear. Under vacuum conditions at 383 K, the sample was dried for 15 h. The resulting sample was the pretreated sample labeled as GAC.

The GAC was crushed into uniform-sized (approximately 2 mm) particles before modification. The GAC particles (1 g or so) were placed in a U-type quartz glass reaction tube fixed in a microwave reactor. First, high-purity $CO_2$ was flushed into the reaction tube at a flow rate of 300 ml·min$^{-1}$ for 20 min. With the $CO_2$ flow equivalent, the microwave reactor (microwave frequency of 2.45 GHz) started irradiating at a power of 0.8 kW for 20 and 40 min. Thereafter, with the microwave maintaining irradiating, high-purity helium was injected into the reaction tube at the same flow rate for 10 min. The microwave reactor was shut down, and the sample was cooled down to room temperature in helium gas atmosphere. The modified activated carbon samples were designated as GAC-20 and GAC-40.

### 2.2. Characterization

The specific surface area and pore structure of the activated carbon samples were evaluated using a Micromeritics ASAP2010 physical adsorption instrument at 77 K in liquid $N_2$. Surface area was calculated according to the standard Brunauer–Emmett–Teller method by using the adsorption data acquired at a relative pressure ($P/P_0$) ranging from 0.05 to 0.25. The microporous specific surface area and volume were calculated by the *t*-plot method. The mesoporous volume was calculated based on the Barrett–Joyner–Halenda (BJH) method. The total pore volume was estimated based on the amount adsorbed at a relative pressure of approximately 0.99. Pore size distribution curves were derived from the analysis of the adsorption branch of the isotherm according to the BJH algorithm [24]. SEM characterization was done using an S4700 field emission scanning electron microscope to observe the apparent morphology of activated carbon, the field emission voltage of which was 15.0 kV. The samples were sprayed *via* gold treatment before the test. The TEM characterization was conducted on Tecnai G2 F30. The sample was dispersed in absolute alcohol and supported on a copper grid before observation. FTIR spectra were obtained by the KBr method, recorded on a Bruker Vector-70, and scanned from 4000 cm$^{-1}$ to 500 cm$^{-1}$. The water contact angles of the samples were measured with a theta optical tensiometer (KSV Instruments) and electro-optics with a closed-circuit television camera connected to a computer (Attension Theta software). A droplet of distilled water (5 μl) was deposited on the surface of the samples. The water contact angle of each sample was measured three times, and the average value was recorded [24].

### 2.3. Adsorption–desorption performance test

The fixed-bed dynamic adsorption–desorption device is shown in Fig. 2. The device was composed of a gas distribution system, an adsorption–desorption fixed-bed system, and a detection system. In the adsorption process, gaseous toluene was generated by bubbling liquid toluene at 273 K with standard air flow. The flow volume was

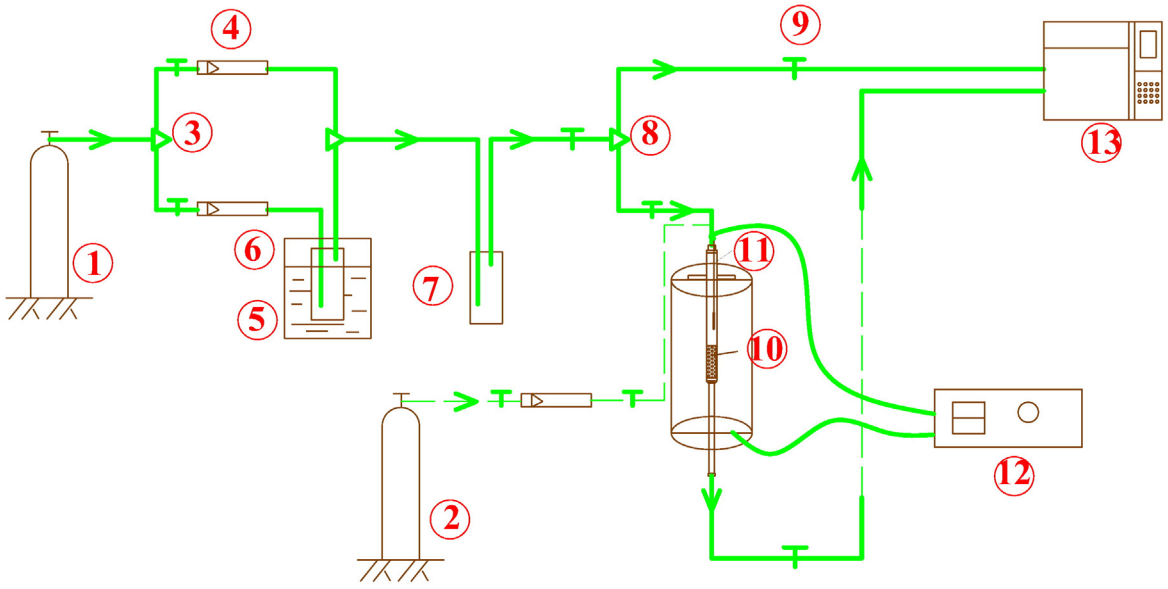


**Fig. 2.** Schematic diagram of experimental apparatus for dynamic absorption and desorption. The solid line represents the adsorption pipe while the dotted line represents the desorption pipe. 1-Standard air cylinder; 2-High purity nitrogen gas cylinder; 3-Tee; 4- Mass flow controller; 5-Thermostatic bath; 6-VOCs generator; 7-Buffer; 8-2-way valve; 9-3-way valve; 10-Reaction tube; 11-K type thermocouple; 12-Temperature programmed control instrument; 13-Agilent GC 6890N.

regulated by a mass flow controller. The generated gaseous toluene was transferred to a buffer by air steam and diluted with air at the required concentration (8214 $mg \cdot m^{-3}$). Before adsorption, gaseous toluene flow (100 $ml \cdot min^{-1}$) was switched into a gas chromatograph (6890N, Agilent Technologies Co., Ltd.) through a three-way valve for detecting gas concentration until stability. Gaseous toluene was passed directly through a sample column at 303 K. The column (8 mm in diameter) was packed with the adsorbent of approximately 0.5 g. The inlet and outlet toluene concentrations were monitored online by the gas chromatograph equipped with a flame ionization detector [24]. In the desorption process, $N_2$ was selected as sweep gas at a flow rate of 20 $ml \cdot min^{-1}$. At the beginning of the desorption process, $N_2$ was purged into the sample column, and the tube furnace was turned on to heat up to 393 K at a heating rate of 10 $K \cdot min^{-1}$. The outlet toluene concentrations were monitored online by the gas chromatograph, and the entire process of desorption lasted for 120 min [25]. The adsorption and desorption capacities were determined by the gravimetric method, *i.e.*, the quality changes of the adsorbent before and after both processes were used to obtain the data of adsorption and desorption capacities.

### 2.4. Determination of adsorption heat

The activated carbon adsorption isotherms of toluene using the dynamic adsorption device were determined. The equilibrium adsorption amount of toluene was measured under six different partial pressures at 303, 318, and 333 K by adjusting the concentration of toluene mixed gas corresponding to different toluene vapor pressures. The Langmuir model can well describe the characteristics of toluene molecules adsorbed on activated carbon at a low pressure. The adsorption process cannot be considered single-molecule-layer adsorption because of the existence of multilayer adsorption and capillary condensation at a high pressure. Therefore, the Langmuir model cannot generate a good fitting effect at a high pressure. For the description of activated carbon and other microporous adsorbents, the Langmuir model can well fit the adsorption process effectively at medium and low pressures [26,27]. In this study, the activated carbon adsorption isotherms of toluene were achieved by nonlinear fitting using the Langmuir isotherm equation. In the medium- and low-pressure sections, the adsorption heat data were calculated by using the Clausius–Clapeyron equation to reflect the change in adsorption intensity before and after modification.

The Langmuir isotherm equation is expressed as follows:

$$\frac{q_e}{q_m} = \frac{KP}{1 + KP}, \tag{1}$$

where $q_e$ is the amount adsorbed at equilibrium ($g \cdot g^{-1}$), $q_m$ is the saturation capacity of the adsorbent ($g \cdot g^{-1}$), $K$ is the Langmuir constant ($m^3 \cdot g^{-1}$), and $P$ is the partial pressure of toluene in air (Pa).

The Clausius–Clapeyron equation can be expressed as follows [28]:

$$\Delta H_s = RT\left(\frac{\partial \ln P}{\partial T}\right)_\Gamma, \tag{2}$$

and its integral form is expressed as follows:

$$\ln P = \text{constant} - \frac{\Delta H_s}{RT}, \tag{3}$$

**Table 1**
Texture parameters of GAC, GAC-20, and GAC-400

| Sample | $S_{BET}/m^2 \cdot g^{-1}$ | $S_{micro}/m^2 \cdot g^{-1}$ | $S_{external}/m^2 \cdot g^{-1}$ | $V_{pore}/cm^3 \cdot g^{-1}$ | $V_{micro}/cm^3 \cdot g^{-1}$ | $V_{meso}/cm^3 \cdot g^{-1}$ | $V_{meso}/V_{pore}$ | $D_{pore}/nm$ |
|---|---|---|---|---|---|---|---|---|
| GAC | 490 | 262 | 228 | 0.254 | 0.132 | 0.122 | 48.03% | 2.1 |
| GAC-20 | 621 | 138 | 483 | 0.351 | 0.081 | 0.270 | 76.92% | 2.3 |
| GAC-40 | 586 | 207 | 379 | 0.324 | 0.121 | 0.203 | 62.65% | 2.2 |

where $\Gamma$ indicates that the adsorption capacity is constant, $\Delta H_s$ is the isosteric adsorption heat ($J \cdot mol^{-1}$), $R$ is the universal gas constant ($8.314\ J \cdot kg^{-1} \cdot K^{-1}$), and $T$ is the temperature (K).

Combined with the Langmuir isotherm equations, the isosteric adsorption heat $\Delta H_s$ was linear fitted using the plot of ln $P$ *versus* $\frac{1}{T}$ and calculated by Eq. (3) at the same equilibrium adsorption amount $q_e$ [29].

## 3. Results and Discussion

### 3.1. Physicochemical and textural characteristics

In the physical activation process of activated carbon with $CO_2$ as an oxidative activation gas, $CO_2$ reacts with the carbon atoms in the active position and the surface active groups of the carbon material to form and

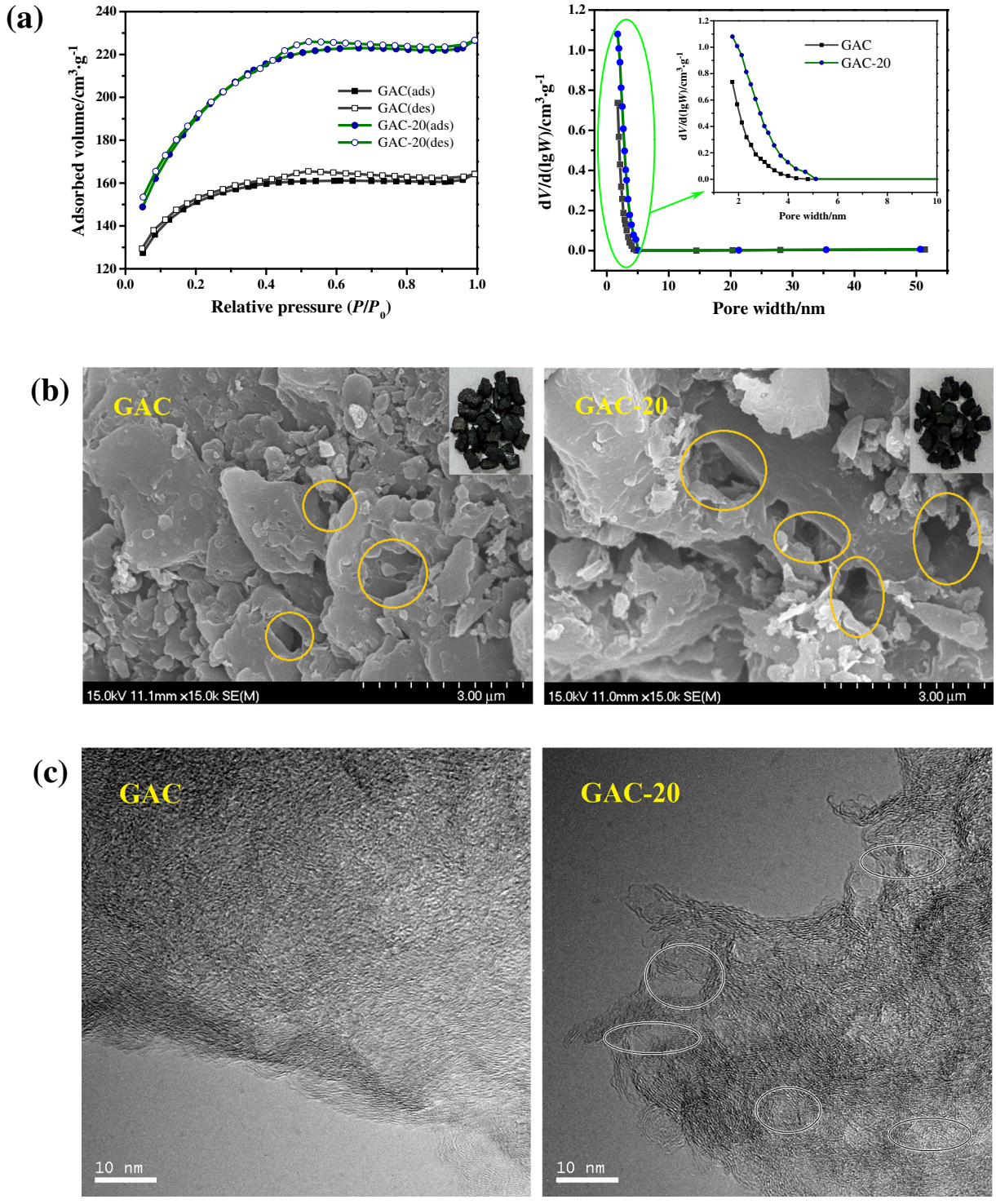


**Fig. 3.** Characterization of texture properties of GAC and GAC-20: (a) $N_2$ absorption–desorption isotherms and pore size distribution; (b) scanning electron microscope (SEM) images; (c) transmission electron microcopy (TEM) images (Ellipse marking areas displaying the microstructure of hierarchical pore formed).

expand the pore structure, which is bound to contain changes in the mass of activated carbon [30,31]. Therefore, the reaction degree of the modification experiments can be determined by the mass loss of GAC. In this experiment, the mass losses of GAC after microwave irradiation for 20 and 40 min were 29.3 and 34.8 $mg \cdot g^{-1}$, respectively. This result indicated that, with the extension of reaction time, the mass loss of activated carbon increased, whereas the yield decreased.

The partially burning loss of functional groups on the surface of activated carbon and the residual volatile matter of the carbon materials in a high-temperature environment will also increase the mass loss of the modified activated carbon [32].

*3.1.1. Textural property characterization*

The physical structure parameters of GAC, GAC-20, and GAC-40 based on $N_2$ adsorption and desorption curves at 77 K are listed in Table 1. The specific surface area $S_{BET}$ and total pore volume $V_{pore}$ of the activated carbon after the $CO_2$/microwave modification treatment were significantly improved. The reason may be the formation of considerable micropores and mesopores and the opening of closed pores [10,23]. The micropore area $S_{micro}$ and micropore volume $V_{micro}$ of GAC-20 and GAC-40 decreased, whereas the specific surface area of mesopores and macropores $S_{external}$ and mesopore volume $V_{meso}$ significantly increased. The mesopore volume of GAC-20 increased from 0.122 $cm^3 \cdot g^{-1}$ to 0.270 $cm^3 \cdot g^{-1}$ compared with that of GAC, indicating that the micropores were expanded and that more mesopores were produced after modification.

Given that GAC-20 showed a better effect on pore expansion after the $CO_2$/microwave modification, GAC and GAC-20 were selected as the follow-up research subjects. The adsorption and desorption studies of nitrogen on GAC and GAC-20 were conducted to characterize their pore structure. The nitrogen adsorption and desorption isotherm curves at 77 K are shown in Fig. 3(a). GAC and GAC-20 exhibited a type I isotherm according to the International Union of Pure and Applied Chemistry (IUPAC) classification (IUPAC, 2015) [33]. In both cases, the nitrogen adsorption isotherms showed three typical steps with the increase in relative pressure. First, at a relative pressure of approximately 0.05, the $N_2$ adsorption amount of the two reached high levels ($>125\ cm^3 \cdot g^{-1}$), indicating that the adsorption curve exhibited a steep increase in the region of low pressure, which represented adsorption or condensation in small micropores. With the increase in relative pressure, the adsorption capacity increased slowly until it reached a "plateau", the stage which represented the progressive filling of larger micropores and mesopores. At this stage, GAC-20 had a greater growth slope, and the "plateau" appeared at a higher relative pressure than that of GAC, indicating that GAC-20 had a more abundant mesopore and a larger micropore volume. Finally, the adsorption amount increased abruptly near the saturation pressure of nitrogen because of active capillary condensation. When the desorption process attached to the intermediate relative pressure section, a type H4 hysteresis loop (IUPAC, 2015) appeared, indicating that GAC and GAC-20 were typically micro–mesoporous materials. The hysteresis loop size of GAC-20 diminished compared with that of GAC, indicating that $N_2$ desorption resistance decreased. The pore size distribution curves based on the BJH method are also shown in Fig. 3(a). After modification, the distribution amount of pore in mesopore size significantly increased, and the right shift of the fall point of GAC-20 was observed, indicating that the distribution width of mesopore increased and that larger mesopores were produced. The average pore size increased from 2.1 nm to 2.3 nm, as shown in Table 1, which indicated that the overall size of the channel became larger, and the effect of pore expansion was obvious.

Fig. 3(b) shows the scanning electron micrographs of GAC and GAC-20 with surface magnification of 15000 times. GAC-20 maintained essentially the same surface topography as that of GAC. The surface structures of GAC and GAC-20 were quite complex, with the surface appearance of folds, irregularities, defects, and richness of macropores, which endowed the activated carbon with excellent adsorption properties.

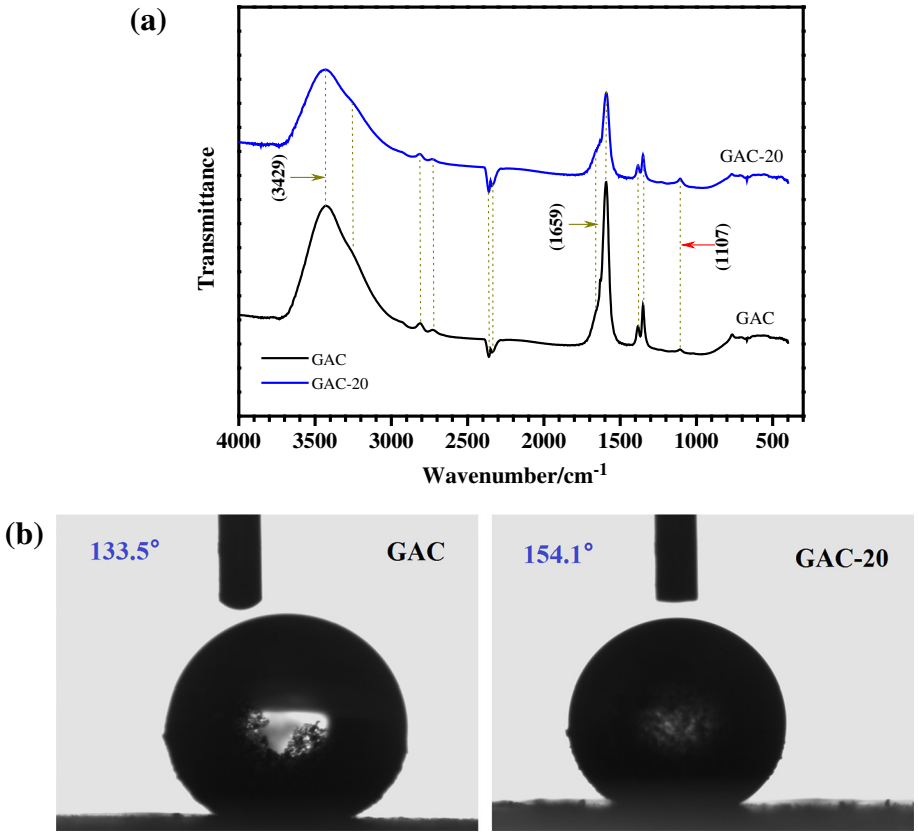


**Fig. 4.** Characterization of surface properties of GAC and GAC-20: (a) Fourier transform infrared spectroscopy (FT-IR) analysis; (b) Water contact angle (photos a water droplet of 5 μl on a tablet of samples).

The basic carbon of activated carbon is composed of graphitized carbon crystallite and ungraphitized non-crystalline carbon. The interaction of non-crystalline carbon and carbon crystallite constitutes the shape and pore structure of the activated carbon. In the activation process of amorphous carbon, organic matters and disordered carbon among the crystal structures are removed to form the pores of activated carbon. GAC and GAC-20 showed a disordered distribution of ordered lamellar carbon crystallite stripes, as revealed by the TEM images shown in Fig. 3(c), which verified the heterogeneous structure of activated carbon [34,35]. The lattice fringes of GAC-20 were clearer and the distribution density was more extensive, indicating that the degree of graphite and the porosity were higher than those of GAC. An irregular pore size between 2 nm and 10 nm in scale can be clearly observed from the TEM of GAC-20, which indicated the formation of hierarchical pore size.

### 3.1.2. Surface property characterization

The FTIR spectra of GAC and GAC-20 are shown in Fig. 4. The graph shows that GAC and GAC-20 had the same peak positions, indicating that no new chemical bonds and functional groups were created after modification. The wide and sharp absorption peaks in 3300 $cm^{-1}$ to 3670 $cm^{-1}$ were attributed to O—H stretching vibration. C═O stretching vibration was observed in 1650 $cm^{-1}$ to 1750 $cm^{-1}$. The weak absorption peak at 1060 $cm^{-1}$ to 1150 $cm^{-1}$ indicated the existence of the asymmetric stretching vibration of C—O—C [35]. After modification, the absorption peak intensity GAC-20 in 3200 $cm^{-1}$ to 3670 $cm^{-1}$ and 1650 $cm^{-1}$ to 1750 $cm^{-1}$ weakened, which indicated that the numbers of hydroxyl (—O—H), carbonyl (—C═O), carboxyl (—COOH), and lactone (—COO) on the activated carbon surface had a certain amount of reduction. Because microwave heating makes high temperature on the surface of activated carbon, than oxygen functional groups were set off thermal cracking reaction. The reduction in phenolic hydroxyl and carboxyl acid groups can decrease the surface acidity of activated carbon. Studies have shown that a decrease in the surface acidity of activated carbon can weaken its adsorption strength to polar molecules [36], which has a positive effect on the desorption of toluene molecules with weak polarity on the activated carbon surface.

To identify the surface hydrophobic properties of the samples, the water contact angles of GAC and GAC-20 were measured and shown in Fig. 4(b). Both samples showed hydrophobic characteristics (*i.e.*, water contact angle over 90°). The contact angle of a water droplet increased from 133.5° to 154.1°, indicating the enhancement of hydrophobicity after modification. Enhanced hydrophobicity may be related to the reduction of hydrophilic groups such as hydroxyl and carboxyl, which is consistent with the previous findings in FTIR spectra.

### 3.2. Dynamic adsorption and desorption

The dynamic adsorption breakthrough curves of GAC and GAC-20 on toluene are shown in Fig. 5(a). The adsorption penetrating time of GAC-20 compared with that of GAC was prolonged by approximately 50 min, which indicated a better adsorption performance. The saturated adsorption capacity of GAC-20 increased from 0.1873 $g \cdot g^{-1}$ to 0.2158 $g \cdot g^{-1}$ compared with that of GAC, and the adsorption performance was significantly improved on account of channel expansion of activated carbon.

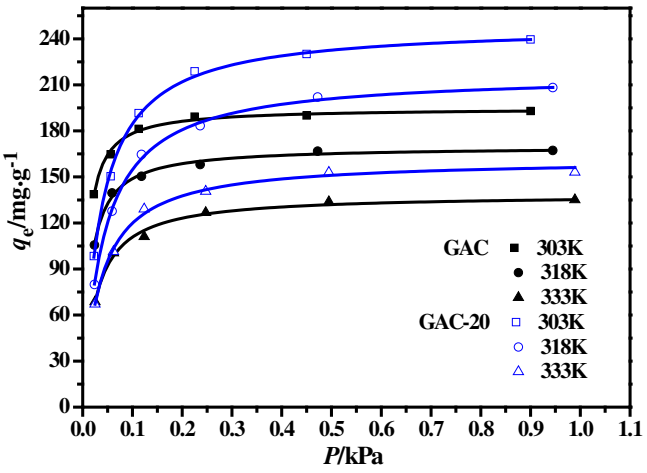


**Fig. 6.** Langmuir isotherm fitting curves of GAC and GAC-20 to toluene at 303 K, 318 K, and 333 K.

The dynamic desorption experiment was conducted on the activated carbon sample-saturated adsorption of toluene at 393 K for 2 h, and the dynamic desorption curves were obtained, as shown in Fig. 5(b). The graph presents that GAC-20 showed a higher instantaneous desorption concentration than that of GAC, and the highest desorption concentration of GAC-20 was higher than that of GAC by approximately 2000 $mg \cdot m^{-3}$. A high instantaneous desorption concentration corresponds to a high desorption rate. The desorption amount and desorption rate of toluene obtained by the weighting method are shown in Table 2. The desorption rate of the modified GAC-20 increased from 69.70% to 78.51%, which was improved by 8.81%, indicating that mesoporous increases contribute to activated carbon desorption for toluene molecules.

**Table 2**
Adsorption and desorption properties of GAC and GAC-20

| Sample | Adsorbent mass/g | Adsorption amount/g | Saturated adsorption amount /$g \cdot g^{-1}$ | Desorption quantity/g | Desorption rate/% |
|---|---|---|---|---|---|
| GAC | 0.5087 | 0.0953 | 0.1873 | 0.0664 | 69.70 |
| GAC-20 | 0.5077 | 0.1095 | 0.2158 | 0.0860 | 78.51 |

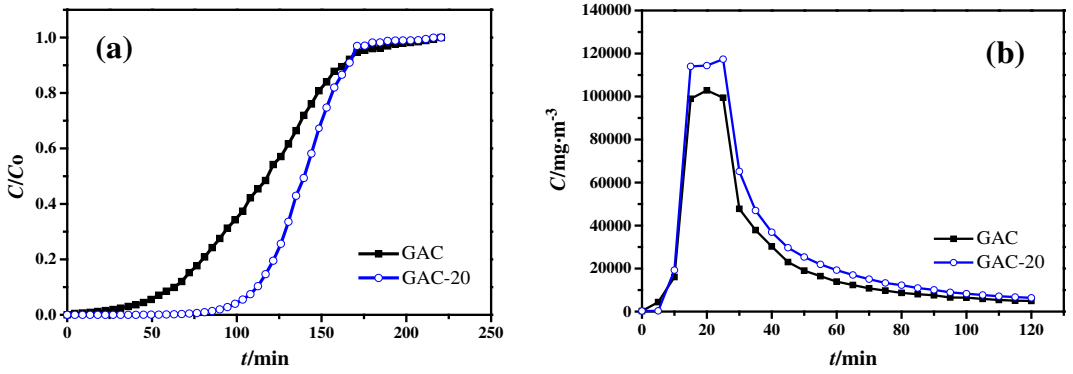


**Fig. 5.** Dynamic adsorption breakthrough curves (a) and desorption curves (b) of GAC and GAC-20; Adsorption conditions: adsorbent (0.5 g), GHSV (12000 $ml \cdot h^{-1} \cdot g^{-1}$), inlet toluene concentration 8214 $mg \cdot m^{-3}$, adsorption temperature (303 K); Desorption conditions: flow volume of $N_2$ (20 $ml \cdot min^{-1}$), desorption temperature (393 K), desorption time (120 min).

**Table 3-1**
Equilibrium adsorption amount of toluene on GAC under different pressures and temperatures

| Serial number | Flow rate $Q$/ml·min$^{-1}$ | GAC | | | | | |
|---|---|---|---|---|---|---|---|
| | | 303 K | | 318 K | | 333 K | |
| | | $P$/kPa | $q_e$/mg·g$^{-1}$ | $P$/kPa | $q_e$/mg·g$^{-1}$ | $P$/kPa | $q_e$/mg·g$^{-1}$ |
| 1 | 50 | 0.0225 | 138.7 | 0.0236 | 105.6 | 0.0247 | 68.7 |
| 2 | 50 | 0.0563 | 164.7 | 0.0590 | 139.6 | 0.0618 | 100.5 |
| 3 | 50 | 0.1125 | 181.3 | 0.1181 | 150.4 | 0.1237 | 111.1 |
| 4 | 50 | 0.2250 | 189.3 | 0.2362 | 158.1 | 0.2473 | 126.8 |
| 5 | 50 | 0.4501 | 190.0 | 0.4723 | 166.8 | 0.4946 | 133.9 |
| 6 | 50 | 0.9001 | 192.9 | 0.9447 | 167.3 | 0.9892 | 135.1 |

**Table 3-2**
Equilibrium adsorption amount of toluene on GAC-20 under different pressures and temperatures

| Serial number | Flow rate $Q$/ml·min$^{-1}$ | GAC-20 | | | | | |
|---|---|---|---|---|---|---|---|
| | | 303 K | | 318 K | | 333 K | |
| | | $P$/kPa | $q_e$/mg·g$^{-1}$ | $P$/kPa | $q_e$/mg·g$^{-1}$ | $P$/kPa | $q_e$/mg·g$^{-1}$ |
| 1 | 50 | 0.0225 | 98.4 | 0.0236 | 79.9 | 0.0247 | 67.1 |
| 2 | 50 | 0.0563 | 150.4 | 0.0590 | 127.7 | 0.0618 | 96.1 |
| 3 | 50 | 0.1125 | 191.6 | 0.1181 | 164.6 | 0.1237 | 108.9 |
| 4 | 50 | 0.2250 | 218.8 | 0.2362 | 183.3 | 0.2473 | 113.4 |
| 5 | 50 | 0.4501 | 230.1 | 0.4723 | 202.0 | 0.4946 | 123.3 |
| 6 | 50 | 0.9001 | 239.6 | 0.9447 | 208.2 | 0.9892 | 126.8 |

### *3.3. Adsorption model and strength*

The isothermal adsorption experiments of GAC and GAC-20 were conducted under different toluene vapor pressures at 303, 318, and 333 K, and their equilibrium adsorption data under different conditions were obtained, as listed in Tables 3-1 and 3-2. The Langmuir isotherm equation was used to fit the equilibrium adsorption data at different temperatures. The fitting curves and parameters are shown and listed in Fig. 6 and Table 4, respectively. The chart shows that the Langmuir simulation results were consistent with the experimental values. The correlation coefficients ($R^2$) were all more than 0.99, indicating that the Langmuir isotherm model was suitable for simulating the adsorption of toluene on GAC and GAC-20.

**Table 4**
Fitting parameters of Langmuir isotherm

| Sample | $T$/K | Langmuir equation | | |
|---|---|---|---|---|
| | | $q_m$/mg·g$^{-1}$ | $K$ | $R^2$ |
| GAC | 303 | 194.9 | 0.1142 | 0.9936 |
| | 318 | 169.8 | 0.0766 | 0.9937 |
| | 333 | 138.6 | 0.0442 | 0.9923 |
| GAC-20 | 303 | 248.8 | 0.0326 | 0.9983 |
| | 318 | 217.2 | 0.0287 | 0.9985 |
| | 333 | 161.6 | 0.0469 | 0.9953 |

Using the isotherm equations under different temperatures determined by the Langmuir isotherm fitting results, we could calculate the corresponding toluene pressure $P$ at 303, 318, and 333 K by integrating the equilibrium adsorption capacity $q_e$ into the isotherm equations at 60, 70, 80, 90, 100, and 110 mg·g$^{-1}$. Then, the isosteric adsorption heat $\Delta H_s$ was linear fitted using the plot of ln $P$ *versus* $1/T$ and calculated by the Clausius–Clapeyron equation (Eq. (3)) [28,29]. The result is shown in Fig. 7. The graph presents that the isosteric heat of adsorption increased nonlinearly with increasing equilibrium adsorption capacity. According to the ideal Langmuir model, the adsorption heat should be independent of coverage [28]. However, in reality, the adsorption heat varies with coverage depending on surface heterogeneity and sorbate–sorbate interaction. The isosteric adsorption heat of GAC-20 decreased by approximately 20 kJ·mol$^{-1}$ after modification, indicating that the heat release of toluene molecules adsorbed on the GAC-20 surface decreased and that the adsorption strength weakened. This finding explained the improvement of desorption efficiency from the view of thermodynamics.

## 4. Conclusions

A method for reactivating activated carbon by $CO_2$/microwave was explored to regulate its pore structure to improve adsorption–desorption performance. In contrast to those of GAC, the adsorption and desorption performances of GAC-20 were significantly improved. The pore size was obviously expanded and the surface active groups

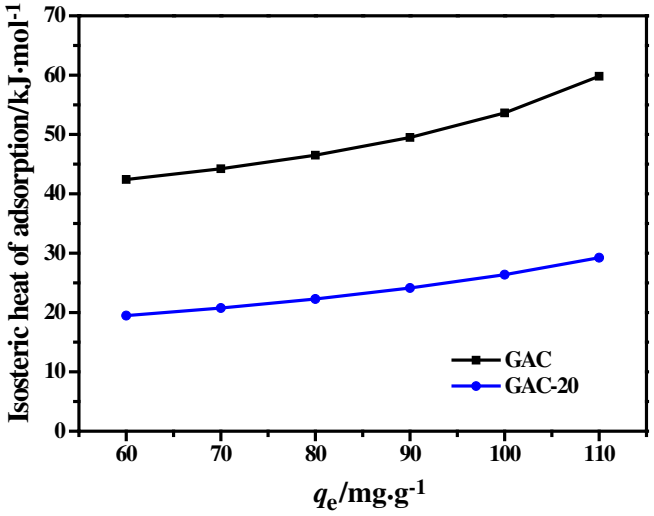


**Fig. 7.** Isosteric adsorption heat curves of GAC and GAC-20 with $q_e$ at 60, 70, 80, 90, 100, and 110 mg·g$^{-1}$.

decreased, which contributed to the desorption of toluene molecules on activated carbon. The Langmuir model can well describe the adsorption of toluene on activated carbon. The isosteric adsorption heat results showed that the adsorption strength of toluene molecules on the modified activated carbon weakened, which can significantly improve the cycle life and stability of activated carbon in practical engineering applications.

## References


[1] T.J. Bandosz, C.O. Ania, Activated carbon surfaces in environmental remediation, *Interface Sci. Technol.* 7 (2006) 159–229.

[2] N. Mohamad Nor, L.C. Lau, K.T. Lee, A.R. Mohamed, Synthesis of activated carbon from lignocellulosic biomass and its applications in air pollution control—A review, *J. Environ. Chem. Eng.* 1 (2013) 658–666.

[3] N. Karatepe, İ. Orbak, R. Yavuz, A. Özyuğuran, Sulfur dioxide adsorption by activated carbons having different textural and chemical properties, *Fuel* 87 (2008) 3207–3215.

[4] R. Pedicini, A. Sacc, A. Carbone, E. Passalacqua, Hydrogen storage based on polymeric material, *Int. J. Hydrog. Energy* 36 (2011) 9062–9068.

[5] H. Yu, K. Zhang, C. Rossi, Theoretical study on photocatalytic oxidation of VOCs using nano-$TiO_2$ photocatalyst, *J. Photochem. Photobiol. A Chem.* 188 (2007) 65–73.

[6] S. Vardharajula, S.Z. Ali, P.M. Tiwari, E. Eroğlu, K. Vig, V.A. Dennis, S.R. Singh, Functionalized carbon nanotubes: Biomedical applications, *Int. J. Nanomedicine* 7 (2012) 5361–5374.

[7] F. Gironi, V. Piemonte, VOCs removal from dilute vapour streams by adsorption onto activated carbon, *Chem. Eng. J.* 172 (2011) 671–677.

[8] T. Dobre, O.C. Pârvulescu, G. Iavorschi, M. Stroescu, A. Stoica, Volatile organic compounds removal from gas streams by adsorption onto activated carbon, *Ind. Eng. Chem. Res.* 53 (2014) 3622–3628.

[9] G.R. Parmar, N.N. Rao, Emerging control technologies for volatile organic compounds, *Crit. Rev. Environ. Sci. Technol.* 39 (2008) 41–78.

[10] K. Yang, J. Peng, C. Srinivasakannan, L. Zhang, H. Xia, X. Duan, Preparation of high surface area activated carbon from coconut shells using microwave heating, *Bioresour. Technol.* 101 (2010) 6163–6169.

[11] D. Das, V. Gaur, N. Verma, Removal of volatile organic compound by activated carbon fiber, *Carbon N. Y.* 42 (2004) 2949–2962.

[12] C. Long, Y. Li, W. Yu, A. Li, Removal of benzene and methyl ethyl ketone vapor: Comparison of hypercrosslinked polymeric adsorbent with activated carbon, *J. Hazard. Mater.* 203-204 (2012) 251–256.

[13] W. Shen, J. Zheng, Z. Qin, J. Wang, Preparation of mesoporous carbon from commercial activated carbon with steam activation in the presence of cerium oxide, *J. Colloid Interface Sci.* 264 (2003) 467–473.

[14] H.M. Williams, E.A. Dawson, P.A. Barnes, G.M.B. Parkes, L.A. Pears, C.J. Hindmarsh, A new low temperature approach to developing mesoporosity in metal-doped carbons for adsorption and catalysis, *J. Porous. Mater.* 16 (2009) 557–564.

[15] A. Oya, S. Yoshida, J. Alcaniz-Monge, A. Linares-Solano, Formation of mesopores in phenolic resin-derived carbon fiber by catalytic activation using cobalt, *Carbon N. Y.* 33 (1995) 1085–1090.

[16] G. Gong, Q. Xie, Y. Zheng, S. Ye, Y. Chen, Regulation of pore size distribution in coal-based activated carbon, *Carbon N. Y.* 47 (2009) 2942.

[17] S. Kang, J. Jian-chun, C. Dan-dan, Preparation of activated carbon with highly developed mesoporous structure from *Camellia oleifera* shell through water vapor gasification and phosphoric acid modification, *Biomass Bioenergy* 35 (2011) 3643–3647.

[18] J. Guo, A.C. Lua, Preparation of activated carbons from oil-palm-stone chars by microwave-induced carbon dioxide activation, *Carbon N. Y.* 38 (2000) 1985–1993.

[19] J. Georgin, G.L. Dotto, M.A. Mazutti, E.L. Foletto, Preparation of activated carbon from peanut shell by conventional pyrolysis and microwave irradiation-pyrolysis to remove organic dyes from aqueous solutions, *J. Environ. Chem. Eng.* 4 (2016) 266–275.

[20] Qing-Song Liu, Tong Zheng, Nan Li, Peng Wang, Gulizhaer Abulikemu, Modification of bamboo-based activated carbon using microwave radiation and its effects on the adsorption of methylene blue, *Appl. Surf. Sci.* 256 (2010) 3309–3315.

[21] A.C. Lua, J. Guo, Activated carbon prepared from oil palm stone by one-step $CO_2$ activation for gaseous pollutant removal, *Carbon N. Y.* 38 (2000) 1089–1097.

[22] S.G. Herawan, M.S. Hadi, M.R. Ayob, A. Putra, Characterization of activated carbons from oil-palm shell by $CO_2$ activation with no holding carbonization temperature, *Sci. World J.* 2013 (2013) 5–7.

[23] F. Rodríguez-Reinoso, M. Molina-Sabio, M.T. González, The use of steam and $CO_2$ as activating agents in the preparation of activated carbons, *Carbon N. Y.* 33 (1995).

[24] H. Feng Lu, J. Jing Cao, Y. Zhou, D. Li Zhan, Y. Fei Chen, Novel hydrophobic PDVB/R-$SiO_2$ for adsorption of volatile organic compounds from highly humid gas stream, *J. Hazard. Mater.* 262 (2013) 83–90.

[25] I.K. Shah, P. Pre, B.J. Alappat, Effect of thermal regeneration of spent activated carbon on volatile organic compound adsorption performances, *J. Taiwan Inst. Chem. Eng.* 45 (2014) 1733–1738.

[26] C.A. Başar, Applicability of the various adsorption models of three dyes adsorption onto activated carbon prepared waste apricot, *J. Hazard. Mater.* 135 (2006) 232–241.

[27] J. Benkhedda, J.N. Jaubert, D. Barth, L. Perrin, Experimental and modeled results describing the adsorption of toluene onto activated carbon, *J. Chem. Eng. Data* 45 (2000) 650–653.

[28] W. Kast, Principles of adsorption and adsorption processes, *Chem. Eng. Process. Process Intensif.* 19 (1985) 118.

[29] S.D. Manjare, A.K. Ghoshal, Adsorption equilibrium studies for ethyl acetate vapor and E-Merck 13X molecular sieve system, *Sep. Purif. Technol.* 51 (2006) 118–125.

[30] R. Okayama, Y. Amano, M. Machida, Effect of nitrogen species on an activated carbon surface on the adsorption of Cu(II) ions from aqueous solution, *Carbon N. Y.* 48 (2010) 45–50.

[31] S. Guo, J. Peng, W. Li, K. Yang, L. Zhang, S. Zhang, H. Xia, Effects of $CO_2$ activation on porous structures of coconut shell-based activated carbons, *Appl. Surf. Sci.* 255 (2009) 8443–8449.

[32] D. Adinata, W.M.A. Wan Daud, M.K. Aroua, Preparation and characterization of activated carbon from palm shell by chemical activation with $K_2CO_3$, *Bioresour. Technol.* 98 (2007) 145–149.

[33] M. East, Physisorption of gases, with special reference to the evaluation of surface area and pore size distribution[J], *Pure & Applied Chemistry* 87 (9) (2015) 25-25, http://dx.doi.org/10.1515/pac-2014-1117.

[34] Y. Liu, L. He, X. Lu, P. Xiao, Transmission electron microscopy study of the microstructure of carbon/carbon composites reinforced with in situ grown carbon nanofibers, *Carbon N. Y.* 50 (2012) 2424–2430.

[35] N. Byamba-Ochir, W.G. Shim, M.S. Balathanigaimani, H. Moon, Highly porous activated carbons prepared from carbon rich Mongolian anthracite by direct NaOH activation, *Appl. Surf. Sci.* 379 (2016) 331–337.

[36] C.C. Huang, H.S. Li, C.H. Chen, Effect of surface acidic oxides of activated carbon on adsorption of ammonia, *J. Hazard. Mater.* 159 (2008) 523–527.